

Molecular Engineering onto Ru^{II} Bis(1,2-diphenylphosphinoethane) Synthons: Toward an Original Organometallic Gelator

Olivier Galangau,* Dania Daou, Nour El Beyrouti, Elsa Caytan, Cristelle Mériadec, Franck Artzner, and Stéphane Rigaut*

Cite This: *Inorg. Chem.* 2021, 60, 11474–11484

Read Online

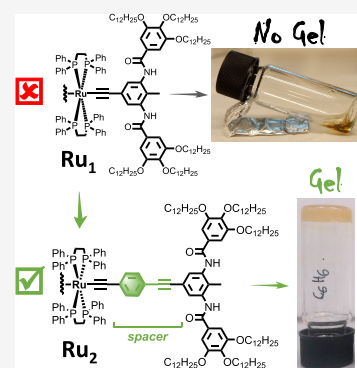
ACCESS |

Metrics & More

Article Recommendations

Supporting Information

ABSTRACT: In this article, we report the successful molecular engineering of Ru bis-acetylides that led for the first time to a gelator and more specifically in aromatic solvents. By means of a nonlinear ligand and an extended aromatic platform, the bulky Ru bis-acetylides were able to self-assemble into lamellar structures as evidenced by scanning electron microscopy (SEM) in benzene, toluene, and *o*- and *m*-xylene, which in turn induced gelation of the solution with a critical gelation concentration of 30 mg/mL. Nuclear magnetic resonance (NMR), variable temperature (VT)-NMR, and Fourier transform infrared (FT-IR) spectroscopies evidenced that hydrogen bonds are mainly responsible for the self-organization. VT-NMR and small-angle X-ray scattering (SAXS) have also suggested that the pro-ligand and the complex stack in different ways.



INTRODUCTION

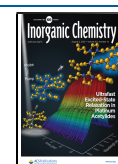
Supramolecular interactions are key features to obtain (multi)functional materials with applications ranging from optoelectronics^{1,2} to molecular electronics.^{3–5} In that regard, molecular gels⁶ have received a great deal of attention in the last decade for their appealing properties that permitted developments of materials with high chemical sensing abilities,^{7–10} remarkable charge transport properties,¹¹ and photochemical and electrochemical responsiveness.^{10,12–14} Gels can be defined as soft materials made of a liquid phase (major component) immobilized in a 3D cross-linked network (minor component). This network can be made of covalent polymeric chains or prepared from the supramolecular assembly of a low-molecular-weight compound, both being known as the gelator. For the so-called supramolecular gels, the gelator self-assembles thanks to a combination of weak interactions such as van der Waals or electrostatic interactions, hydrogen/halogen bonding, and/or π – π stacking interactions. A gel is commonly identified by the test inversion method that consists of looking at the ability of the soft material to support its own weight when the vial is turned upside down. Therefore, a gel can be interpreted as a clear sign of self-assembly properties, whereas the lack of gelation may stem from a limited propensity to form supramolecular polymers. Recently, metallogels^{15–18} where the gelator is either a coordination or an organometallic complex have drawn a lot of attention. Indeed, the presence of the metal has brought about new features such as redox responses,¹⁹ luminescence,²⁰ or catalytic activities.²¹ They have also found applications in waveguiding²² or for anticancer treatment.²³ Among all metal-

logelators, rigid rod-like metal-acetylides, where the metal is Pt(II)^{24–27} or Au(III),²⁸ are efficient gelators thanks to their flat structures and, for Pt(II) centers, their ability to provide additional metal–metal interactions^{29,30} that are further driving the supramolecular assembly. Because of their photophysical properties, those metal-acetylide metallogels/gelators were mainly used as light-emitting soft materials. Alternatively, metallogels transporting electrical charges are well desired for the development of flexible, lightweight electronic devices, although examples have been scarcely documented so far.³¹ To obtain rigid-rod conductive supramolecular metallogels, organometallic acetylides gelators must combine strong supramolecular association with reversible redox processes at low potentials.

Our group, among others, has been involved in the chemistry of mono- and bimetallic Ru(II) bis-acetylide complexes holding great promises for optoelectronic applications. Indeed, these compounds feature remarkable charge transport properties in nanojunctions,^{32–41} on gold surfaces as charge storage layer,⁴² or as “push–pull” chromophoric reagents for solar cells⁴³ and NLO applications.^{44–48} Recently, we also reported Ru bis-acetylides as efficient electrochemical switches for lanthanide emission in the NIR ranges^{49,50} or

Received: May 17, 2021

Published: July 22, 2021

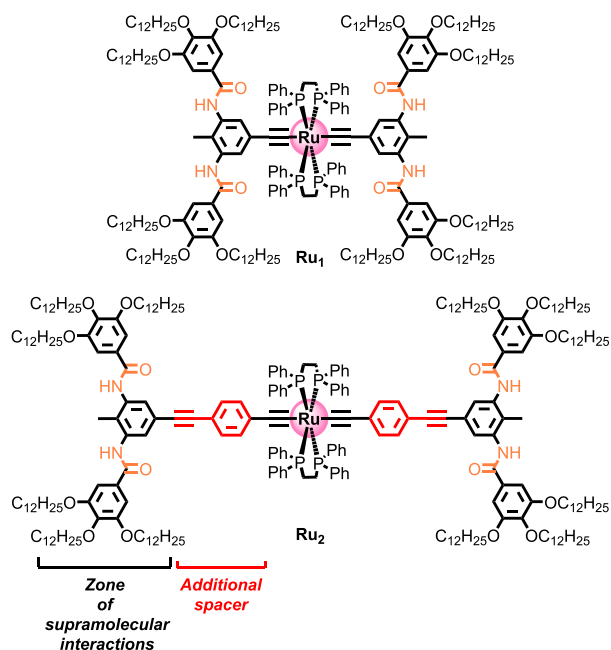


magnetic properties.⁵¹ However, to the best of our knowledge, there is no example of mono- or bimetallic Ru(II) bis-acetylide derivatives able to form supramolecular assemblies/gels, which would widen their application field to charge transport properties on long distances, thanks to their unique electronic properties. This statement presumably results from the fact that the stabilizing *1,2-dppe* ancillary ligands prevent accurate intermolecular contacts.⁵² Therefore, designing Ru(II) bis-acetylide complexes able to overcome this drawback and form supramolecular architectures accommodating their bulky ligands is challenging.

We anticipated that placing an acetylide ligand, featuring a simple hydrogen donating/accepting moiety in *trans* position with respect to the metal center, would not be sufficient for driving self-assembly as it is for Pt(II) bis-acetylide²² derivatives. Therefore, we selected a ligand that could trigger the gelation of alkane solvents, while connected to a bulky coordination sphere, such as those used in the Ln(III) complexes developed by Ziesel, Camerel, and Charbonnière.^{53,54} This ligand encompasses a central toluyl fragment connected to two amide functions that, on the basis of crystallographic data, was found to pack in a head-to-tail fashion with a molecular packing driven by hydrogen bonding interactions. The toluyl fragment is essential since it prevents the amide functions from planarizing (see [Supporting Information](#)).

This article will disclose the synthesis and the physicochemical properties of two original symmetrical monometallic Ru(II) bis-acetylide complexes featuring this efficient platform ([Chart 1](#)). It was also found that **Ru₂**, which encompasses an

Chart 1. Molecular Structures of Ru₁ and Ru₂ Complexes

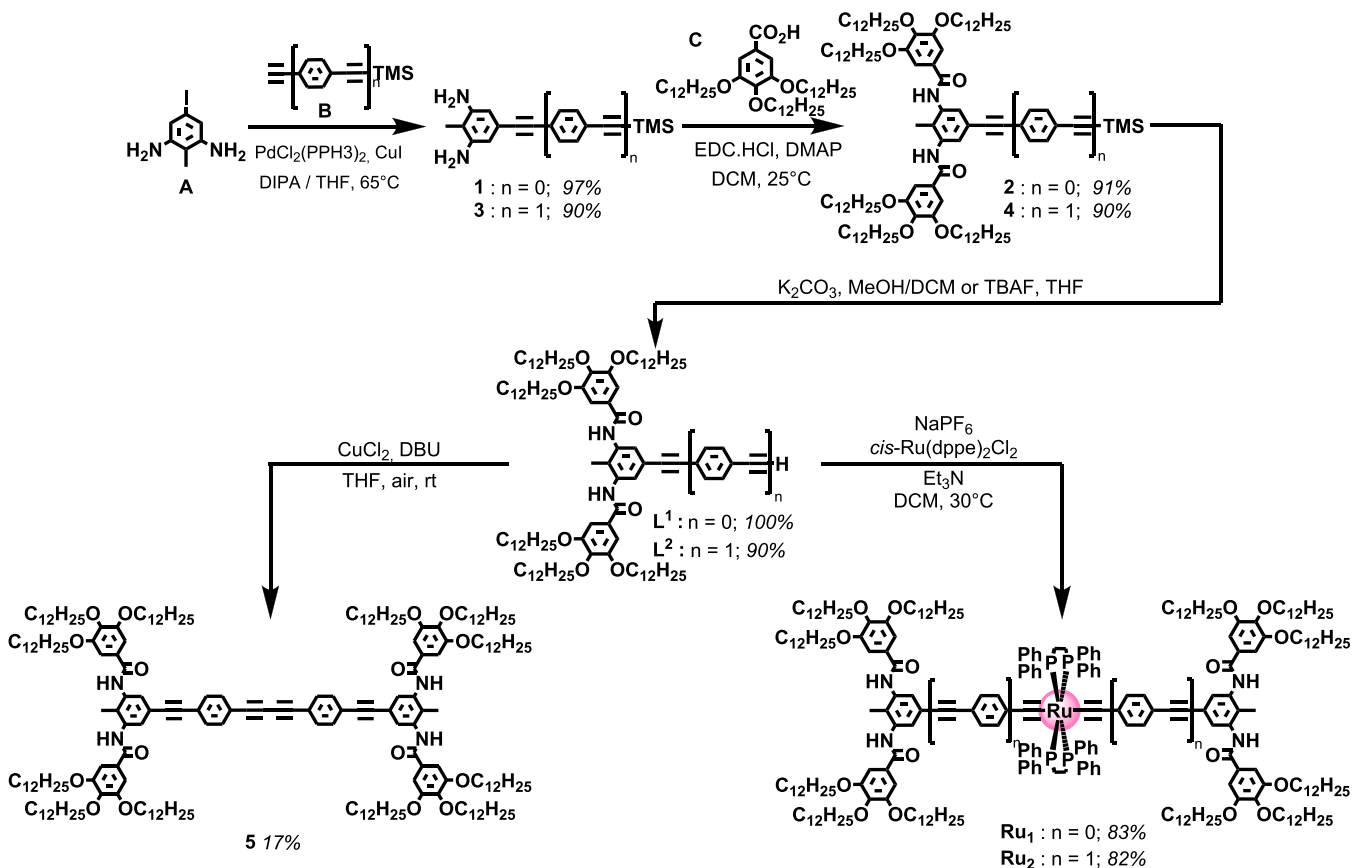


extended ligand aiming at further separating the hydrogen bonding sites from the *1,2-dppe* crowded unit and favoring additional π - π stacking interactions, affords organogels in aromatic solvents.

RESULTS AND DISCUSSIONS

Syntheses. **Ru₁** and **Ru₂** derivatives were obtained from a multistep synthetic procedure in very good yields ([Scheme 1](#)). Both compounds are air- and bench-stable yellow powders. The starting compound **A** was converted into compound **I** through Sonogashira coupling (97%). Aniline functional groups of **I** were further coupled to the gallic acid **C** presenting three dodecyl alkyl chains, with mild conditions, to afford the intermediate derivative **2** (91%). Finally, deprotection of the TMS group of **2** afforded **L¹** quantitatively. A similar synthetic path was chosen for preparing **L²**. The difference lies in the first step. Compound **A** was coupled to derivative **B** featuring a TMS-protected phenyl acetylene moiety to yield intermediate **3** in a quantitative manner. Note that **L¹** and **L²** are stable for months, at room temperature and under air. Finally, **Ru₁** and **Ru₂** complexes were obtained in 83 and 82% yields, respectively, in the presence of NaPF₆/Et₃N.⁵⁵ The temperature was maintained at 30 °C to ensure the proper solubility of the pro-ligands. These Ru complexes were characterized with ¹H, ¹³C, ³¹P, and FT-IR spectroscopies and HR-MS, and TGA proved their thermal stability up to 300 °C ([Figure S40](#)). Spectrophotometric properties of **Ru₁** and **Ru₂** were studied in DCM (see [Figure S47](#) and [Table S4](#)). **Ru₁** displays classically two main absorption bands located at 267 and 338 nm, and **Ru₂** presents two redshifted absorption bands, with maxima positioned at 280 and 402 nm. On the basis of TDDFT calculations (see [Supporting Information](#)), we ascribed for **Ru₁** the transition at 338 nm to a $d/\pi \rightarrow \pi^*$ located on the *dppe* and the acetylide fragments, while for **Ru₂**, the transition at 402 nm was ascribed to a $d/\pi \rightarrow \pi^*$ involving the acetylide fragments only. We have also probed their electrochemical behavior. Both compounds undergo a fully reversible one-electron oxidation process at around 0.4 V vs SCE in DCM (0.2 M ⁿBu₄NPF₆) at room temperature as we expected ([Supporting Information](#)). Finally, we also prepared compound **5**, which does not present the Ru-centered building block, to investigate the importance of the molecule rod-like shape. As a result, derivative **5** was obtained from the homocoupling of **L²** under Glaser conditions in poor yields (17%). This low yield probably originates from the very poor solubility of **5** in common organic solvents that prevent high yield purification.

Gelation Properties. The gelation properties of **L²**, **Ru₁**, **Ru₂**, and **5** studied by the inversion method are summarized in [Table 1](#). The pro-ligand **L²** was able to form transparent gels ([Figure 1](#)) in alkane solvents such as cyclohexane, methylcyclohexane, *n*-dodecane, or *n*-heptane with a CGC (critical gelation concentration) of 1.3 mg/mL, except for methylcyclohexane (4.0 mg/mL). These values are similarly to those found for other organic gelators possessing an analogous structure.⁵⁴ As previously reported by Ziesel et al.,⁵⁶ **L¹** affords turbid gels in acetone only. Therefore, extending the aromatic platform with **L²** has markedly improved the overall gelation ability. Interestingly, gelation abilities are annihilated with dimer compound **5** as it is not soluble in any solvents used in this study, except in CHCl₃ that was used to characterize it. Concerning the complexes, **Ru₁** does not form any gels but precipitates in cyclohexane and methylcyclohexane when cooling down to room temperature. In aromatic solvents, the molecule is still soluble after cooling. On the contrary, the **Ru₂** derivative affords turbid gels in aromatic solvents, while in alkanes, the compound is not soluble. CGCs of approxima-

Scheme 1. Synthetic Routes to Compounds L^1 , L^2 , Ru_1 and Ru_2 Table 1. Summary of Gelation Properties^a

	Cy	MeCy	<i>n</i> -heptane	<i>n</i> -dodecane	benzene	toluene	<i>o</i> -xylene	<i>m</i> -xylene
L_2	G (1.3)	G (4.0)	G (1.3)	G (1.4)	NS	NS	NS	NS
5	NS	NS	NS	NS	NS	NS	NS	NS
Ru_1	P	P	NS	NS	S	S	S	S
Ru_2	NS	NS	NS	NS	G (30)	G (20)	G (30)	G (33)

^aNumbers in bracket represent the critical gelation concentration given in mg/mL. G = gel, P = precipitate after cooling down, NS = not soluble, and S = soluble after cooling down (no gel).

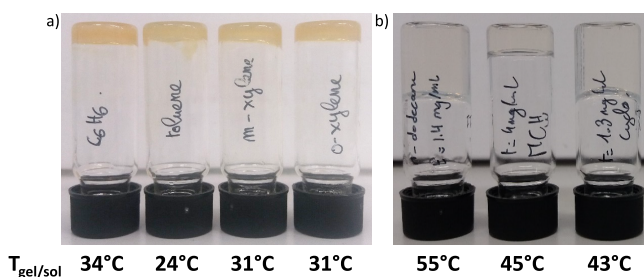


Figure 1. Pictures of gels from (a) Ru_2 and (b) L^2 derivatives. Gel-to-solution transition temperatures are indicated at the bottom of the figure.

tively 30 mg/mL were obtained for benzene and *o*- and *m*-xylene, while a CGC of 20 mg/mL was measured for toluene. When compared to the best organic gelator found in the literature (CGC < 1 mg/mL), Ru_2 gelation aptitudes are moderate but comparable to those of other acetylide complexes. For example, in 2011, Yang's group reported a series of bimetallic Pt(II) bis-acetylide complexes featuring an

iptycene as the central bulky fragment.⁵⁷ Unexpectedly, these molecules formed gels in alkanes with CGCs ranging from 20 to 65 mg/mL. In the present case, Ru_2 is the first example of its kind providing organogels despite having such a sterically highly demanding ancillary ligand. Furthermore, comparing compounds **5** and Ru_2 indicates that the *dppe* ligands play a key role in solubilizing the organometallic molecule in aromatic solvents. We have also measured the gel-to-solution transition temperatures by immersing the samples in a temperature-controlled bath. Transition temperature refers to the temperature at which the gel (at the CGC) starts to melt and collapses when the tube is turned upside down. Regarding pro-ligand L^2 , transition temperatures of 55 °C were found in *n*-heptane and *n*-dodecane, whereas values of 43 and 45 °C were obtained in cyclohexane and methylcyclohexane, respectively. As a result, gels of L^2 in linear alkanes are more robust than those in cyclic ones. Gels of Ru_2 in aromatic solvents display transition temperatures of 24 °C in toluene, 31 °C in *o*- and *m*-xylene, and 34 °C in benzene.

Gels of Ru_2 and of L^2 are stable for at least 2 months in usual laboratory conditions. Even after this period of time, the

gelation process can be repeated at least 5–10 times with no apparent loss of efficiency. Note that these gels do not show any thixotropic behavior. In short, comparison between derivatives L^2 , Ru_1 , and Ru_2 clearly demonstrates the importance of (i) the $1,2$ -*dppe* ligand that brings about some solubility and gelling ability in aromatic solvents, and (ii) extending the aromatic surface to favor self-assembly, which probably overcomes the steric hindrance provided by the *dppe* crown, leading to more available hydrogen bonding sites and extending the aromatic platform to offer more possibilities for the molecules to pack thanks to π - π stacking interactions in particular in L^2 (*vide infra*). Comparing Ru_1 and Ru_2 1H NMR spectra in CD_2Cl_2 where no supramolecular interactions take place (see Supporting Information), we observed that, at room temperature, the signal assigned to aromatic protons located on the tolyl fragment experiences a drastic downfield shift from Ru_1 to Ru_2 (from 6.80 to 7.70 ppm), while the hydrogen atoms located on the gallate moieties are not affected. This shift evidences the magnetic influence of the *dppe* crown on these protons. Moreover, signals attributed to the methyl and the amide protons are also similarly influenced by the *dppe* to a minor extent. Therefore, it is reasonable to think that, in Ru_1 , the supramolecular packing of the ligand *via* hydrogen bonding and π - π stacking is prevented because of the bulkiness of the ancillary ligand, which in turn explains why it does not afford gels in aromatic solvent while Ru_2 does (*vide infra*). This result sheds light on the importance of the ligand design and on the importance of the *dppe* crowding.

To further support this statement, we have transposed to our complexes the model of Cavallo et al., originally developed for a better understanding of catalytic activities of organometallic complexes.⁵⁸ Cavallo's calculations provide (i) the percentage of buried volumes, i.e., the space occupied by a ligand in the first coordination sphere of a metal center or a putative atom, and (ii) the corresponding topographic steric map of a ligand. Consequently, this map provides a quantitative description of the interaction surface between the spherical center and a substrate. Assuming that the approach of a "substrate" could be regarded as a supramolecular overlap, calculating the buried volume (steric map) at a judiciously chosen point along the molecular axis is highly relevant to apprehend the steric bulk of the *dppe* units and the possibilities of interactions in the present case. To achieve these calculations, we first simulated Ru_1 and Ru_2 geometries with a DFT method (see Supporting Information for more details). Then, we used these results to calculate Cavallo's parameters for a putative atom located at the center of the tolyl fragment along the Ru_1 and Ru_2 long molecular axis. In Ru_2 , the percentage of buried volume (% V_{bur}) is calculated to be 0%, reflecting a free environment available for supramolecular interactions, while in Ru_1 , at the same location, % V_{bur} is found to be 23%, indicating that the *dppe* chelate probably precludes ligand overlapping and further supramolecular interactions.

In the next sections, we now describe our further studies on the morphologies of the gels and xerogels by scanning electron microscopy and FT-IR.

Scanning Electron Microscopy and FT-IR Studies (SEM). SEM was performed to study the morphology of the corresponding xerogels (freeze-dried gels) of compounds L^2 and Ru_2 . As observed in Figure 2, a 3D network comprising entangled fibers was obtained for the xerogel of L^2 , with fiber diameters of 100–300 nm. In contrast, Ru_2 presents flat ribbons with widths of approximately 200–400 nm, along

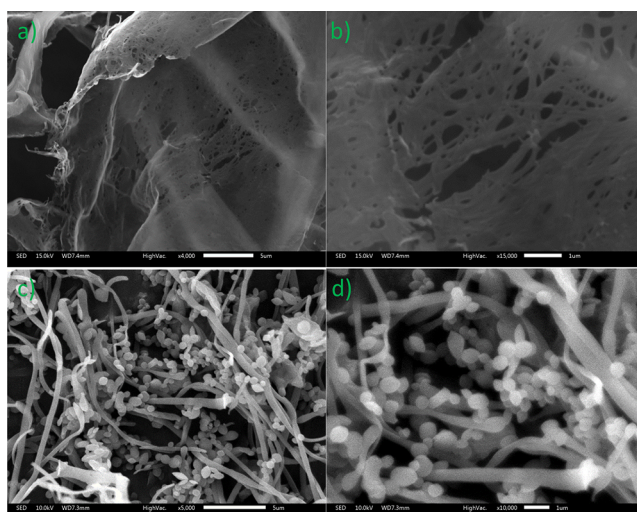


Figure 2. SEM images of xerogels of L^2 in cyclohexane, CGC = 1.3 mg/mL (a) scale bar at 5 μ m and (b) scale bar at 1 μ m. SEM images of xerogels of Ru_2 in benzene, CGC = 30 mg/mL (c) scale bar at 5 μ m and (d) scale bar at 1 μ m.

with spherical particles with diameters ranging from 200 to 1000 nm. The origin of the presence of two different types of supramolecular objects remains elusive so far. Spherical particles might be due to self-aggregation during the freeze-drying step. Nevertheless, these SEM experiments prove the capability of compound Ru_2 to self-assemble into supramolecular ribbons. The FT-IR spectrum of these xerogels displays the vibration of the amide C=O bond at 1635 cm^{-1} for L^2 and 1637 cm^{-1} for Ru_2 (Figure 3). In addition, the N—

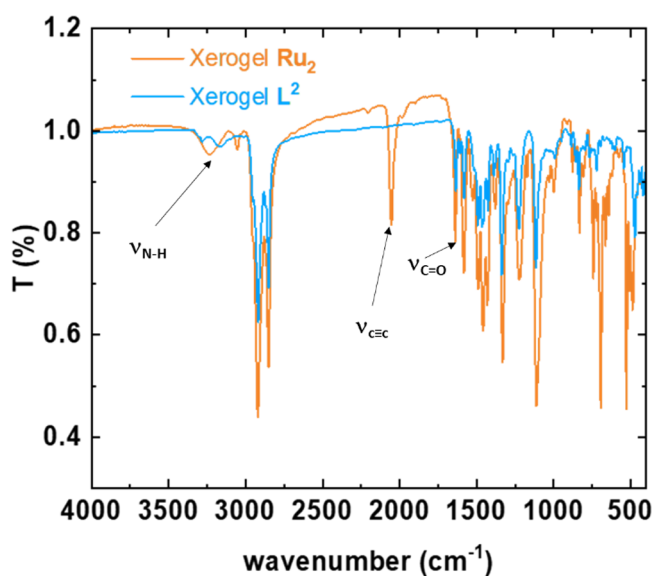
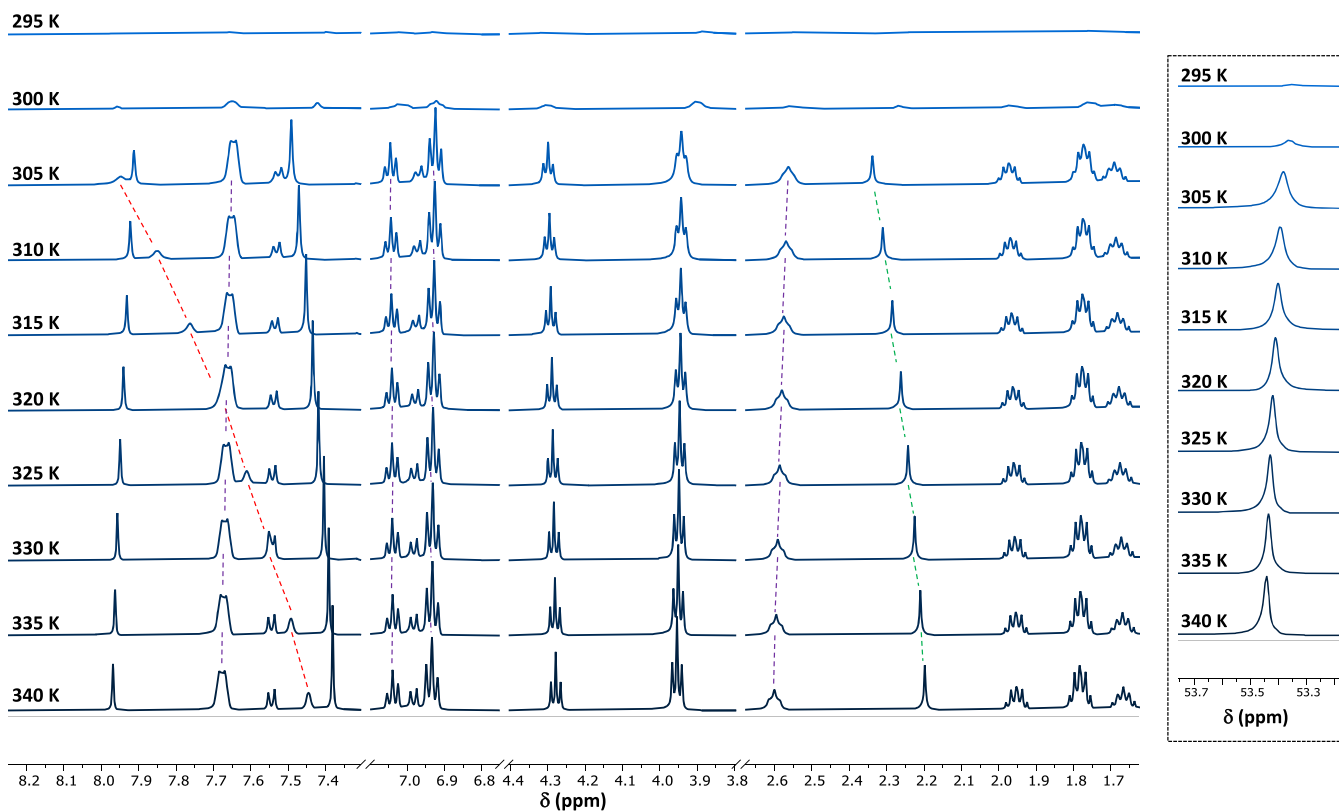


Figure 3. Xerogel FT-IR spectrum of L^2 in cyclohexane, CGC = 1.3 mg/mL, and of Ru_2 in benzene, CGC = 30 mg/mL.

H vibration from the amido moieties was found at 3153 cm^{-1} for L^2 and 3230 cm^{-1} for Ru_2 . These values are characteristic of hydrogen-bonded molecules and are close to values found for a very similar molecular skeleton.⁵⁴

NMR Studies of Gelation. To get more insight into the supramolecular processes, the gel formation was monitored by 1H variable temperature NMR (VT-NMR) studies in C_6D_{12}

Scheme 2. Partial ^1H VT-NMR Monitoring of Ru_2 in C_6D_6 ($c = 30 \text{ mg/mL}$)^a

^aInset shows $^{31}\text{P}\{^1\text{H}\}$ VT-NMR monitoring recorded in the same conditions. Lines are used as guide for the eye. Red line = amide protons, green line = methyl signal, and purple line = 1,2-*dppe* signals.

for L^2 and C_6D_6 for Ru_2 . Starting with compound L^2 (see Supporting Information), the broad signal located at 8.3 ppm assigned to amide group protons experiences a downfield shift (+0.61 ppm) as the temperature decreases from 340 to 320 K. This is a clear evidence of the involvement of the hydrogen bonds into the supramolecular process as indicated in the xerogel with IR spectroscopy. Interestingly, aromatic signals experience an upfield shift as well as the methyl protons' signal located at 2.00 ppm (−0.13 ppm). Finally, the alkynyl proton exhibits no shift, which leads us to think that this part of the molecule is not involved in the supramolecular packing. Additional 2D ROESY experiment performed at 325 K features a cross-correlation between the alkynyl proton and some protons from the aliphatic chains (Figure S29), which proves that these two groups of atoms are spatially close during the self-assembly process. These observations are consistent with a head-to-tail supramolecular assembly as previously suggested by Ziessel et al. on an analogous system (see Supporting Information).⁵⁴ As far as the Ru_2 derivative is concerned, we have conducted ^1H and ^{31}P VT-NMR experiments in C_6D_6 at the CGC (Scheme 2). First, the $^{31}\text{P}\{^1\text{H}\}$ experiment displays one singlet signal located at approx. 53.5 ppm at 340 K, a value that is characteristic of a Ru(II) *trans*-bis-acetylide complex. By slowly cooling down the sample to 295 K, the singlet signal undergoes a slight shift and vanishes because of gelation at 300 K. This singlet signal reappears when the sample is warmed above the gelation temperature. We repeated this experiment at least four times and showed great reproducibility with no obvious degradation. Therefore, we can safely conclude that Ru_2 is chemically stable in that temperature range, as already

suggested by qualitative observations. Regarding the ^1H NMR spectrum, the broad singlet signal located at 7.45 ppm and assigned to amide protons experiences a significant downfield shift from 340 to 300 K (+0.55 ppm). This is in line with molecules interacting through hydrogen bonds, presumably between their amide groups, as for L^2 . Importantly, the singlet signal located at 2.20 ppm (methyl protons) also experiences a downfield shift. This is in stark contrast with what was observed on ligand L^2 and might suggest, at this stage, that Ru_2 does not pack the same way as L^2 does. However, the choice of solvent deeply matters in the context of supramolecular chemistry, and therefore, the comparison between L^2 and Ru_2 may not be so straightforward.⁵⁹ Interestingly, multiplet signals due to the *dppe* aromatic protons do not shift with temperature, indicating that the *dppe* is not involved in the supramolecular process, as we anticipated. Additional 2D NOESY and 2D ROESY performed at 315 K exhibit cross-correlations indicating several dipolar couplings between protons of the toluyl fragment, the amido groups, and the fatty chains (Figures S30 and S31). These through-space couplings support the existence of supramolecular contacts involving the acetylide ligands. Further variable temperature DOSY-NMR (Figure S29) was conducted in C_6D_6 at the CGC to measure the gel-to-solution transition temperature. The molecular diffusion coefficient decreased with temperature before reaching a plateau at 32 °C, meaning that the gel state was obtained. This value is in good agreement with the one measured previously (Figure 1).

To sum up, experiments that combined FT-IR with NMR and VT-NMR have clearly established that hydrogen bonds are

involved in the construction of the supramolecular assemblies. On one hand, L^2 seems to behave as reported by Ziesel et al., with molecules packing in a head-to-tail fashion and rejecting the alkyne protons out of the structure. On the other hand, whereas the Ru_2 compound also exhibits hydrogen bonding that is central for the assembly (downfield shift of the amide proton signal), the methyl signal also experiences a downfield shift that is inconsistent with a head-to-tail supramolecular packing. Eventually, VT-NMR, 2D NOESY, and 2D ROESY clearly evidence that *dppe* is not involved in the supramolecular process.

Small-Angle X-ray Scattering (SAXS). To get a better insight into the supramolecular architectures of both gels, we performed small-angle X-ray scattering experiments. The X-ray scattering of the ligand L^2 (Figure 4) exhibits two peaks at

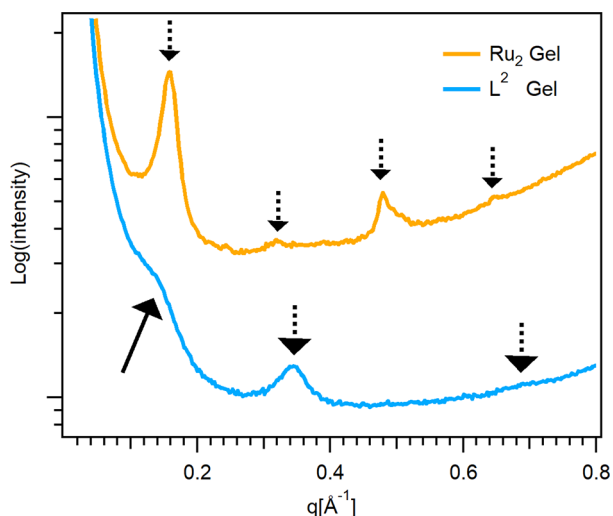


Figure 4. SAXS diffractogram of L^2 and Ru_2 collected in gels at their respective CGC. Patterns are shifted for clarity. Dotted arrows correspond to lamellar peaks. The solid line indicates a lateral order within the layers.

0.344 and 0.69 \AA^{-1} corresponding to long-range order with a lamellar repeat distance a_L of 18.2 \AA (Supporting Information, Figure 5). An additional broad scattering is observed at 0.15 \AA^{-1} indicating a short-range order interdistance b_L of $42 \pm 5 \text{\AA}$. This suggests a lamellocolumnar organization. In this hypothesis, the columnar cross section is $S_L = a_L \times b_L = 760 \text{\AA}^2$. These arrangements and surface are close to those of the parent system⁵⁴ and confirm the column formation tendency observed by NMR and FT-IR. Note that the orientation of the diamido backbone can be either in-plane or perpendicular to the layer. However, this can be clarified by noting that the aromatic volume ratio is between 25 and 30%. This imposes the mean thickness of the aromatic part in the lamellar structure to be thinner than 5.5 \AA , which is incompatible with a perpendicular orientation. The in-plane orientation is compatible with observed H-bonds and the head-to-tail packing hypothesis. Thus, the hierarchical structure of the gel is consequently formed by large fibers that are made of columns with a head-to-tail packing organized in layers by means of chain interdigitation.

The X-ray scattering of Ru_2 (Figure 4) exhibits a well-defined set of lamellar peaks at 0.158, 0.32, 0.48, and 0.65 \AA^{-1} corresponding to a repeat distance a_{Ru} of 39.2 \AA . The length of the aromatic-ethenyl-Ru rigid part is about 33 \AA . This is compatible with a perpendicular orientation to the layers. Interestingly, the amide backbone is parallel to the layer and therefore perpendicular to the mean plane containing the acetylide scaffold. In other words, Ru_2 forms lateral intermolecular hydrogen bonds leading to layers of molecules showing a segregation between the aliphatic part and the aromatic part. Thanks to chain interdigitations, the layers assemble together affording large ribbons (Figure 5) responsible for the gelation. In particular, aromatic solvent molecules might be confined within the layers, therefore contributing to the overall solvent immobilization. Such a result echoes with the fact that the Ru_2 gels are weak, are fragile, and feature moderate gel-to-sol transition temperatures. Overall, SAXS confirms that L^2 and Ru_2 present different packing as already suggested by the VT-NMR experiments.

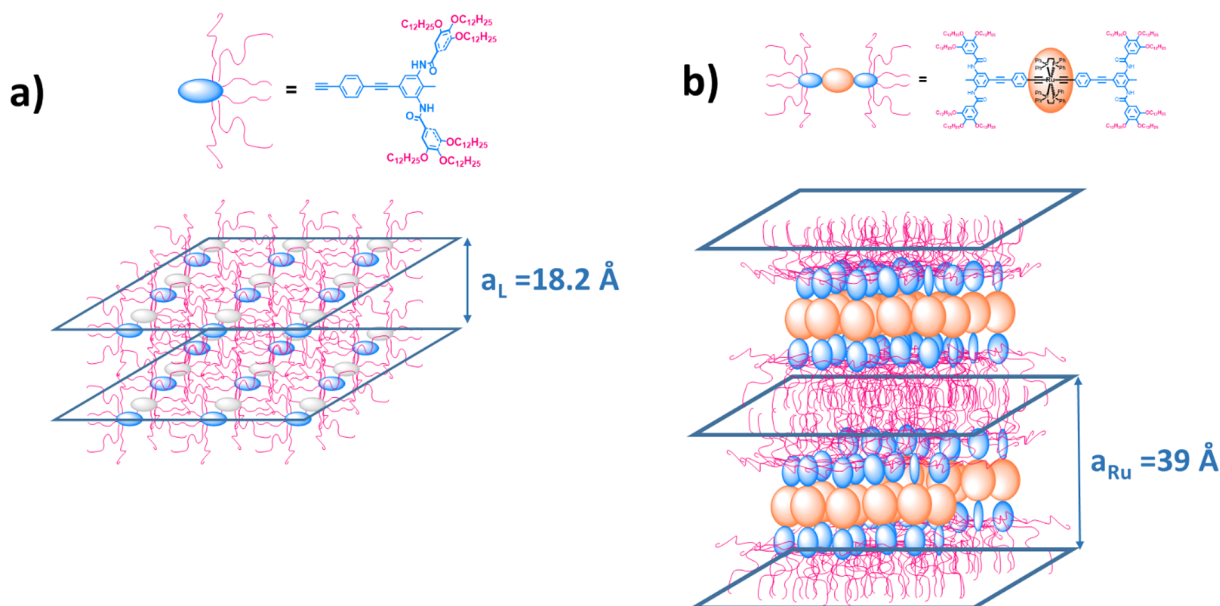


Figure 5. Schematic of the internal structure of (a) L^2 fibers and (b) Ru_2 ribbons according to the SAXS data.

CONCLUSIONS

To conclude, we have successfully synthesized the first example of a Ru(II) bis-acetylide complex showing supramolecular capabilities. By means of a rational molecular engineering that consists of (i) placing hydrogen bonding accepting/donating groups out of the molecule's long axis and (ii) extending the ligand platform to decrease the steric influence of the *dppe* crown, this complex was able to form ribbons in aromatic solvents, which in turn induced gelation of the solution. In particular, NMR, VT-NMR, and FT-IR spectroscopies have evidenced that hydrogen bonds are mainly responsible for the self-organization. VT-NMR and SAXS have also suggested that both the pro-ligand and the complex self-assemble thanks to hydrogen bonding interactions. While L^2 packs in a head-to-tail fashion, Ru_2 forms lateral hydrogen bonding with a segregation between the aliphatic and the aromatic parts. We are currently investigating the self-assembly mechanism and the necessity for the complex to be symmetrical to generate supramolecular packing. We believe that these results open the door to new opportunities for redox active Ru bis-acetylide compounds and will encourage the development of new parent complexes featuring improved gelation efficiencies.

EXPERIMENTAL SECTION

General Information. Chemicals and solvents (HPLC, spectroscopic grade) were purchased from Merck-Sigma Aldrich, Acros Organics, Alfa Aesar, and Fisher Scientific and were used without any further treatment. Anhydrous (HPLC) solvents were obtained from a MBraun SPS-800 drying system. Dry THF was obtained after distillation on Na/benzophenone. Dry diisopropylamine (DIPA), dry triethylamine (TEA), and dry DMF were obtained after distillation on CaH_2 and kept in the dark on molecular sieves. All reactions were carried out under an argon atmosphere using Schlenk techniques, unless otherwise stated. Schlenk tubes were dried under vacuum using a heat gun. TLC analyses were achieved on silica gel bought from Fluka (silica gel matrix containing a fluorescent indicator at 254 nm). Column chromatography was performed on silica gel from Acros Organics (pore size of 60 Å, particle size of 40–63 μ m), unless otherwise stated. 1H , ^{13}C , and ^{31}P -NMR spectra were recorded on a Bruker Avance III (400 MHz) and Bruker AMX-300 (300 MHz) at 303 K. Relevant compounds were also characterized by 2D NMR using HSQC/HMQC, COSY 1H - 1H , and HMBC sequences. VT-NMR was recorded on a Bruker Ascend 500 MHz Av III HD. Deuterated solvents were bought from Euriso-top. Infrared spectra (KBr) were acquired on an FT-IR BRUKER EQUINOX 55 spectrophotometer. HR-MS spectra were obtained from the Centre Régional de Mesures Physiques de l'Ouest (CRMPO). Intermediate **A** was obtained through an adapted procedure from the literature (see Supporting Information). Precursors **B** and **C** were synthesized as reported in the literature (see Supporting Information for reference).

Thermogravimetric Analyses. TGA curves were recorded on a TGA-DSC 1 STAR System under a nitrogen atmosphere.

Electrochemical Measurements. Electrochemical studies were carried out under argon using an Eco Chemie Autolab PGSTAT 30 potentiostat (CH_2Cl_2 , 0.2 M Bu_4NPF_6); the working electrode was a carbon disk and decamethylferrocene was the internal reference.

Scanning Electron Microscopy (SEM). Metallization by Au/Pd. Scanning electron microscopy (SEM) of xerogels was evaluated using the JEOL IT 300 scanning electron microscope. Samples were collected and deposited on a Teflon plot. Each sample was examined using a voltage of 5 or 10 kV. Images were analyzed by the SMileView software.

Small-Angle X-ray Scattering (SAXS). Organogel and xerogel samples were prepared inside capillaries. SAXS experiments were performed using X-ray patterns collected with a Pilatus 300k (Dectris, Grenoble, France) mounted on a GeniX 3D (Xenocs, Sassenage, France) microsource X-ray generator operating at 30 W. The

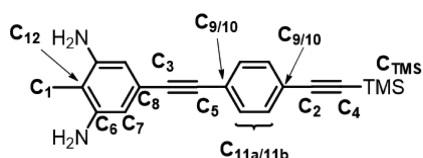
monochromatic Cu $K\alpha$ radiation is of $\lambda = 1.541$ Å. The diffraction patterns were therefore recorded for reciprocal spacing $q = 4\pi \times \sin\theta/\lambda$ in a range of repetitive distances from 0.015 Å $^{-1}$ (418 Å) to 1.77 Å $^{-1}$ (8 Å). Images were transformed to graphics using a home-developed program.

SYNTHESES

Compound 1. A dried Schlenk tube was charged with compound **A** (0.200 g, 0.8 mmol, 1 eq.), $PdCl_2(PPh_3)_2$ (0.085 g, 5 mol %), and CuI (0.023 g, 5 mol %) under argon flow. Then, distilled Et_3N (12 mL) was added followed by dry THF (12 mL). To this mixture was added the excess of neat TMSA (500 μ L, 5 mmol, 2 eq.), and the mixture was refluxed for 24 h. The crude was allowed to cool to room temperature and was diluted with aq. NH_4Cl saturated solution. The aqueous layer was extracted with $EtOAc$ several times. The organics were dried over Na_2SO_4 and filtered, and the solvents were removed. The crude mixture was purified by flash column chromatography (silica, DCM/ $EtOH$ 0 to 1.2%) to afford 512 mg of the expected compound **1** (yield 97%). 1H NMR (400 MHz, $CDCl_3$): $\delta = 6.33$ (s, $2H_{Ar}$), 3.53 (broad singlet, $4H_{amine}$), 1.95 (s, $3H_{methyl}$), 0.22 (s, $9H_{TMS}$); ^{13}C NMR (100 MHz, $CDCl_3$): $\delta = 144.84, 120.92, 110.25, 108.47, 105.74, 92.08, 10.31, 0.02$ (C_{TMS}). HRMS (ESI): m/z 219.1312 calcd for $C_{12}H_{19}N_2Si$ [$M + H^+$]; found: 219.1312.

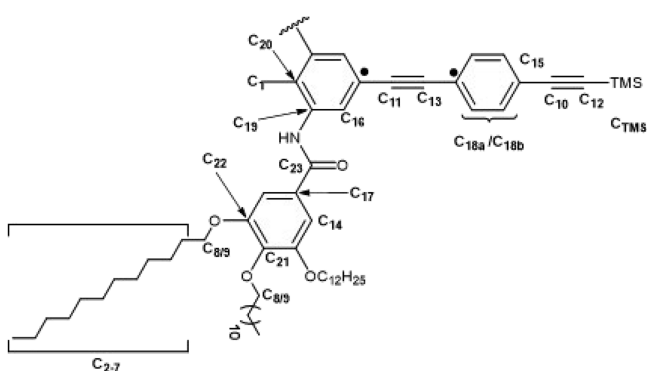
Compound Ru_1 . A dried Schlenk flask was charged with *cis*- $RuCl_2(dppe)_2$ (0.050 g, 0.05 mmol, 1 eq.), compound **L**¹ (0.165 g, 0.11 mmol, 2.2 eq.), and $NaPF_6$ (0.052 g, 0.31 mmol, 6 eq.) under argon flow. The tube was evacuated (30 min) and backfilled with argon. Then, a solution of distilled Et_3N (417 μ L, 3 mmol, 60 eq.) in dry DCM (16 mL) was added with a syringe. The reaction mixture was stirred at 30 °C during 4 days. $^{31}P\{^1H\}$ (no lock procedure) NMR monitoring of the reaction indicated only one singlet signal at around 53 ppm. The reaction mixture was diluted with DCM (10 mL) and washed with water (3×10 mL). The organic layer was collected, dried on Na_2SO_4 , and filtered, and the solvent was removed. The crude was taken up in 10 mL of DCM and precipitated by dropwise addition of 10 mL of MeOH. The yellow precipitate was filtered off under air and dried to afford the corresponding Ru_1 compound ($m = 0.164$ g, yield 83%). 1H NMR (400 MHz, CD_2Cl_2): $\delta = 7.51$ (m, 20H $H_{dppe} + H_{amide}$), 7.49 (t, 16H, $^3J_{HH} = 7.6$ Hz, H_{dppe}), 7.13–7.17 (m, 16H, $H_{Ar} + H_{dppe}$), 6.81 (s, 4H, H_{tol}), 4.08 (dt, 24H, $^3J_{HH} = 6.5$ Hz, H_{alkyl}), 2.66 (br. s, 8H, CH_2_{dppe}), 2.17 (s, 6H, H_{Me}), 1.88–1.71 (m, 28H, H_{chain}), 1.54 (m, H_{chain}), 1.28 (br. s, 205H, H_{chain}), 0.88 (m, 36H, Me_{chain}); ^{13}C NMR (75 MHz, CD_2Cl_2): $\delta = 166.09, 153.75, 141.68, 141.68, 137.46$ (quint, $J = 10.2$ Hz), 136.27, 134.61, 130.43, 129.09, 127.57, 125.24, 123.13, 116.07, 73.93, 69.82, 32.39, 31.85 (m, $^1J_{P,C} + ^3J_{P,C} = 24$ Hz, $P(CH_2)_2P$), 30.81, 30.21–29.81 (br. m.), 26.59, 23.14, 23.12, 14.32, 13.13. $^{31}P\{^1H\}$ NMR (162 MHz, CD_2Cl_2): $\delta = 53.17$. HRMS (ESI): m/z 3814.6316 calcd for $C_{242}H_{370}N_4O_{16}P_4$ ^{102}Ru [M^+]; found 3814.6298. IR (cm^{-1}): 3255 (ν_{N-H}), 2912, 2851 (ν_{C-H}), 2051 ($\nu_{C \equiv C}$), 1639 ($\nu_{C=O}$), 1582 ($\nu_{C=C}$). λ_{max} (solvent, ϵ): 338 nm (DCM, 38000 L mol $^{-1}$ cm $^{-1}$).

Compound 3. A dried Schlenk tube was charged with compound **A** (0.200 g, 0.8 mmol, 1 eq.), compound **B** (0.208 g, 1.0 mmol, 1.3 eq.), $PdCl_2(PPh_3)_2$ (0.028 g, 5 mol %), and CuI (0.007 g, 5 mol %) under argon flow. Dry THF (4 mL) and dry DIPA (4 mL) were added by a syringe. The mixture darkened. The dark solution was refluxed (65 °C) for 24 h. The crude was diluted with saturated aq. NH_4Cl solution and



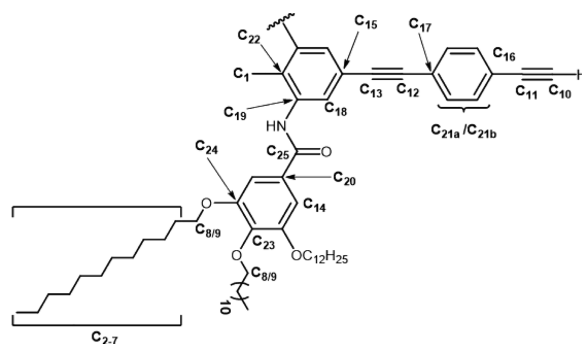
extracted with Et₂O several times. The organics were combined, dried over MgSO₄, and filtered, and the solvents were removed. Purification by column chromatography (silica, DCM/EtOAc mixture) afforded the desired compound **3** (*m* = 0.230 g, yield 90%). ¹H NMR (400 MHz, CDCl₃): δ = 7.42 (s, 4H, H_{10/11}), 6.38 (s, 2H, H₇), 3.59 (broad singlet, 4H, H_{amine}), 1.97 (s, 3H, H₁), 0.26 (s, 9H, H_{TMS}); ¹³C NMR (100 MHz, CDCl₃): δ = 145.09 (C₁₂), 131.78 (C_{11b}), 131.28 (C_{11a}), 123.69 (C₁₀), 122.47 (C₉), 120.77 (C₈), 109.73 (C₇), 108.35 (C₆), 104.73 (C₅), 95.98 (C₄), 91.99 (C₃), 87.35 (C₂), 10.33 (C₁), -0.09 (C_{TMS}). HRMS (ESI): *m/z* 341.1445 calcd for C₂₀H₂₂N₂Si Na [M + Na⁺]; found: 341.1445.

Compound 4. A dried Schlenk tube was charged with compound **3** (0.164 g, 0.52 mmol, 1 eq.), compound **C** (0.870



g, 1.3 mmol, 2.5 eq.), EDC-HCl (0.248 g, 1.3 mmol, 2.5 eq.), and DMAP (0.157 g, 1.3 mmol, 2.5 eq.) under argon flow. Dry DCM (3.5 mL) was added via a syringe. The brownish solution was then warmed at 30 °C over 3 days. The crude was diluted with DCM and washed with water. The organic phase was collected, dried on Na₂SO₄, and filtered. The solvent was removed. Purification by column chromatography (silica, DCM/EtOAc 100%/0% to 98%/2%) afforded the desired compound (*m* = 0.671 g, yield 80%). ¹H NMR (400 MHz, CDCl₃): δ = 7.74 (s, 2H₁₆), 7.65 (br. s, 2H, H_{amide}), 7.42 (s, 4H, H₁₈), 7.09 (s, 4H, H₁₄), 4.04 (m, 12H, H₈), 2.25 (s, 3H, H₁), 1.83 (m, 12H, H₂₋₇), 1.43–1.23 (m, 108H, H₂₋₇), 0.88 (m, 18H, H₂₋₇), 0.25 (s, 9H, H_{TMS}); ¹³C NMR (75 MHz, CDCl₃): δ = 165.94 (C₂₃), 153.28 (C₂₂), 141.77 (C₂₁), 139.67 (C₂₀), 136.43 (C₁₉), 131.83 (C_{18b}), 131.32 (C_{18a}), 128.99 (C₁₇), 125.42 (C₁₆), 123.05 (C₁₅), 123.00 (C₁₄), 106.02 (C₁₃), 104.61 (C₁₂), 96.25 (C₁₁), 90.45 (C₁₀), 89.45 (C_{8/9}), 73.59 (C_{8/9}), 69.44 (C₇), 31.92 (C₆), 30.36 (C₅), 29.75 (C₅), 29.71 (C₅), 29.66 (C₅), 29.61 (C₅), 29.44 (C₅), 29.36 (C₅), 26.11 (C₄), 22.68 (C₃), 14.09 (C₂), 13.36 (C₁), -0.10 (C_{TMS}). HRMS (MALDI-DCTB): *m/z* 1654.293 calcd for C₁₀₆H₁₇₄N₂O₈SiNa [M + Na⁺]; found: 1654.282. IR (cm⁻¹): 3177 (ν_{N-H}), 2917 (ν_{C-H}), 2850 (ν_{C-H}), 2109 (ν_{C=C}), 1635 (ν_{C=O}), 1580 (ν_{C=C}).

Compound L². A round-bottom flask equipped with a magnetic stirring bar was charged with compound **4** (0.671 g, 0.41 mmol, 1 eq.). The compound was dissolved in a 1/1 (v/v) DCM and MeOH (total volume of 30 mL) at room temperature. Then, K₂CO₃ (2.552 g, 18.5 mmol, 45 eq.) was



added, and the suspension was stirred 4–5 h. The mixture was partitioned between water and DCM. The aqueous layer was extracted several times with DCM. The organic phase was dried on MgSO₄ and filtered, and the solvents were removed to afford a light yellowish powder with enough purity to be used for the next step (0.635 g, yield 99%). ¹H NMR (300 MHz, CDCl₃): δ = 7.98 (s, 2H, H_{amide}), 7.59 (s, 2H, H₁₈), 7.41 (d, 2H, ³J_{HH} = 8.2 Hz, H₂₁), 7.33 (d, 2H, ³J_{HH} = 8.2 Hz, H₂₁), 7.14 (s, 4H, H₁₄), 4.02 (m, 12H, H_{8/9}), 3.15 (s, 1H, H_{alkyne}), 2.17 (s, 3H, H₁), 1.80 (m, 12H, H₆), 1.47–1.27 (m, 108H, H_{4/5}), 0.88 (m, 18H, H₂); ¹³C NMR (75 MHz, CDCl₃): δ = 165.96 (C₂₅), 153.26 (C₂₄), 141.70 (C₂₃), 136.40 (C₂₂), 131.99 (C_{21b}), 131.39 (C_{21a}), 128.94 (C₂₀), 127.69 (C₁₉), 125.51 (C₁₈), 123.45 (C₁₇), 121.93 (C₁₆), 121.08 (C₁₅), 105.96 (C₁₄), 90.51 (C₁₃), 89.23 (C₁₂), 83.20 (C₁₁), 78.88 (C₁₀), 73.57 (C₉), 69.40 (C₈), 31.92 (C₇), 30.36 (C₆), 29.76 (C₅), 29.66 (C₅), 29.45 (C₅), 29.37 (C₅), 29.36 (C₅), 26.12 (C₄), 22.68 (C₃), 14.10 (C₂), 13.38 (C₁). HRMS (ESI): *m/z* 1582.2536 calcd for C₁₀₃H₁₆₆N₂O₈Na [M + Na⁺]; found: 1582.2543. IR (cm⁻¹): 3442 (ν_{N-H}), 3288 (ν_{CC-H}), 2916 (ν_{C-H}), 2852 (ν_{C-H}), 2107 (ν_{C=C}), 1635 (ν_{C=O}), 1583 (ν_{C=C}).

Compound 5. A round-bottom flask equipped with a magnetic stirring bar was charged with compound **L²** (0.448 g, 1 mmol, 1 eq.), anhydrous CuCl₂ (0.004 g, 0.0287 mmol 0.1 eq.), and THF (6 mL). Neat DBU was added dropwise (0.051 mL, 0.34 mmol, 1.2 eq.). The mixture was refluxed over 1 day with no precaution to remove air. The reaction mixture was taken to dryness. Purification by column chromatography (Florisil, PE/CHCl₃ (9/1, v/v) to CHCl₃) followed by precipitation in a mixture of CHCl₃ and MeOH afforded the pure compound **5** (*m* = 0.150 g, yield 17%). ¹H NMR (400 MHz, CDCl₃): δ = 7.90 (s, 4H, H_{amide}), 7.64 (s, 4H, H_{Ar tol}), 7.44 (d, 4H, ³J_{HH} = 8.3 Hz, H_{Ar acetylene}), 7.37 (d, 4H, ³J_{HH} = 8.3 Hz, H_{Ar acetylene}), 7.12 (s, 8H, H_{Ar side}), 4.02 (m, 24H, H_{Omethylen}), 2.20 (s, 6H, H_{Methyl}), 1.81 (m, 24H, H_{chain}), 1.47–1.26 (m, 216H, H_{chain}), 0.88 (m, 36H, H_{chain}); ¹³C NMR (75 MHz, CDCl₃): δ = 166.07, 153.24, 141.73, 136.40, 132.32, 131.48, 128.91, 128.13, 125.83, 123.90, 121.45, 121.05, 106.06, 91.28, 89.35, 82.01, 75.72, 73.56, 69.41, 31.82, 30.38, 29.76, 29.67, 29.47, 29.37, 26.13, 22.68, 14.08, 13.36. HRMS (ESI): *m/z* 3139.5024 calcd for C₂₀₆H₃₃₀N₄O₁₆Na [M + Na⁺]; found: 3139.5007. IR (cm⁻¹): 3181 (ν_{N-H}), 2916 (ν_{C-H}), 2054 (ν_{C-H}), 1636 (ν_{C=O}), 1583 (ν_{C=C}).

Compound Ru₂. A dried Schlenk flask was charged with *cis*-RuCl₂(dppe)₂ (0.121 g, 0.13 mmol, 1 eq.), compound **L²** (0.400 g, 0.26 mmol, 2.05 eq.), and NaPF₆ (0.122 g, 0.73 mmol, 5.8 eq.) under argon flow. The tube was evacuated and backfilled with argon. Then, a solution of distilled Et₃N in dry DCM (16 mL) was added. Finally, the reaction mixture was warmed at 30 °C during 4 days. ³¹P{¹H} (no lock procedure) NMR monitoring indicated only one singlet signal at 52.8

ppm. The reaction was stopped by adding 20 mL of MeOH over 20 min. The compound was filtered off. The powder was taken up in DCM (20 mL) and precipitated with MeOH (8 mL) to afford pure compound **Ru₂** as a yellow powder (*m* = 0.412 g, yield 82%). ¹H NMR (400 MHz, CD₂Cl₂): δ = 7.74 (s, 4H, H_{amide}), 7.73 (s, 4H, H_{tol}), 7.49 (m, 16H, H_{dppe}), 7.30 (d, 4H, ³J_{HH} = 8.3 Hz, H_{Ar acetylene}), 7.20 (s, 8H, ³J_{HH} = 7.5 Hz, H_{dppe}), 6.97 (t, 16H, ³J_{HH} = 7.7 Hz, H_{dppe}), 6.72 (d, 4H, ³J_{HH} = 8.4 Hz, H_{Ar acetylene}), 4.04 (dt, 24H, ³J_{HH} = 6.6 Hz, H_{Omethylene}), 2.66 (br. s, 8H, H_{dppe}), 2.25 (s, 6H, H_{Me}), 1.88–1.71 (m, 28H, H_{aliphatic}), 1.54 (m, H_{aliphatic}), 1.28 (br. s, 205H, H_{aliphatic}), 0.88 (m, 36H, H_{aliphatic}); ¹³C NMR (75 MHz, CD₂Cl₂): δ = 165.91, 153.27, 141.47, 137.17, 137.00, 136.87, 136.69, 134.10, 130.89, 130.76, 129.99, 129.83, 129.23, 128.74, 127.77, 125.29, 121.72, 117.63, 116.58, 105.82, 90.93, 88.53, 73.49, 69.37, 31.94, 31.38 (m, ¹J_{P,C} + ³J_{P,C} = 24 Hz, P(CH₂)₂P), 30.40, 29.77–29.38 (br. m.), 26.16, 22.69, 13.87, 13.24. ³¹P{¹H} NMR (162 MHz, CD₂Cl₂): δ = 52.89. HRMS (ESI): *m/z* 1338.2312 calcd for C₂₅₈H₃₇₈N₄O₁₆P₄¹⁰²Ru [M³⁺]; found: 1338.2321. IR (cm⁻¹): 3432 (ν_{N-H}), 2921 (ν_{C-H}), 2054 (ν_{C≡C}), 1636 (ν_{C=O}), 1583 (ν_{C=C}). λ_{max} (ε): 402 nm (solvent = DCM, 63000 L mol⁻¹ cm⁻¹).

■ ASSOCIATED CONTENT

Supporting Information

The Supporting Information is available free of charge at <https://pubs.acs.org/doi/10.1021/acs.inorgchem.1c01488>.

Precursor synthetic procedures; NMR spectra of **L²**, **S**, **Ru₁**, and **Ru₂**; comparative NMR studies of **Ru₁** and **Ru₂** in CD₂Cl₂; VT-NMR monitoring for compounds **L²** and **Ru₂**; gel formation procedure and corresponding summary of the gel properties; SEM images; absorption spectrum of **Ru₁** and **Ru₂**; CV of **Ru₁** and **Ru₂**; and DFT and TDDFT calculations for **Ru₁** and **Ru₂** (PDF)

■ AUTHOR INFORMATION

Corresponding Authors

Olivier Galangau – Univ Rennes, CNRS, ISCR (Institut des Sciences Chimiques de Rennes)-UMR 6226, Rennes F-35000, France; Email: olivier.galangau@univ-rennes1.fr

Stéphane Rigaut – Univ Rennes, CNRS, ISCR (Institut des Sciences Chimiques de Rennes)-UMR 6226, Rennes F-35000, France; orcid.org/0000-0001-7001-9039; Email: stephane.rigaut@univ-rennes1.fr

Authors

Dania Daou – Univ Rennes, CNRS, ISCR (Institut des Sciences Chimiques de Rennes)-UMR 6226, Rennes F-35000, France

Nour El Beyrouiti – Univ Rennes, CNRS, ISCR (Institut des Sciences Chimiques de Rennes)-UMR 6226, Rennes F-35000, France

Elsa Caytan – Univ Rennes, CNRS, ISCR (Institut des Sciences Chimiques de Rennes)-UMR 6226, Rennes F-35000, France; orcid.org/0000-0003-0490-3074

Cristelle Mériadec – Univ Rennes, CNRS, IPR (Institut de Physique de Rennes)-UMR 6251, Rennes F-35000, France

Franck Artzner – Univ Rennes, CNRS, IPR (Institut de Physique de Rennes)-UMR 6251, Rennes F-35000, France

Complete contact information is available at:

<https://pubs.acs.org/doi/10.1021/acs.inorgchem.1c01488>

Notes

The authors declare no competing financial interest.

■ ACKNOWLEDGMENTS

The authors thank the Université de Rennes 1 and the CNRS for the support. The authors are grateful to Dr. Camerel for the fruitful discussions about the gel formation. This work was granted access to the computing resources of CINES (Montpellier, allocation 2019-A0060810728 and 2020-AP010811752 awarded by GENCI). The authors also thank F. Gouttefangeas and L. Joanny from the CMEBA (Centre de Microscopie Electronique à Balayage et microAnalyse, Rennes) for assistance in recording SEM images.

■ REFERENCES

- (1) Amabilino, D. B.; Smith, D. K.; Steed, J. W. Supramolecular materials. *Chem. Soc. Rev.* **2017**, *46*, 2404–2420.
- (2) Li, Q.; Li, Z. Molecular Packing: Another Key Point for the Performance of Organic and Polymeric Optoelectronic Materials. *Acc. Chem. Res.* **2020**, *53*, 962–973.
- (3) Hasegawa, M.; Iyoda, M. Conducting supramolecular nanofibers and nanorods. *Chem. Soc. Rev.* **2010**, *39*, 2420–2427.
- (4) Wang, S.; Kappl, M.; Liebewirth, I.; Muller, M.; Kirchhoff, K.; Pisula, W.; Mullen, K. Organic field-effect transistors based on highly ordered single polymer fibers. *Adv. Mater.* **2012**, *24*, 417–420.
- (5) Faramarzi, V.; Niess, F.; Moulin, E.; Maaloum, M.; Dayen, J. F.; Beaufrand, J. B.; Zanettini, S.; Douidin, B.; Giuseppone, N. Light-triggered self-construction of supramolecular organic nanowires as metallic interconnects. *Nat. Chem.* **2012**, *4*, 485–490.
- (6) Weiss, R. G. The past, present, and future of molecular gels. What is the status of the field, and where is it going? *J. Am. Chem. Soc.* **2014**, *136*, 7519–7530.
- (7) Kartha, K. K.; Babu, S. S.; Srinivasan, S.; Ajayaghosh, A. Attogram sensing of trinitrotoluene with a self-assembled molecular gelator. *J. Am. Chem. Soc.* **2012**, *134*, 4834–4841.
- (8) Babu, S. S.; Praveen, V. K.; Ajayaghosh, A. Functional π-gelators and their applications. *Chem. Rev.* **2014**, *114*, 1973–2129.
- (9) Babu, S. S.; Prasanthkumar, S.; Ajayaghosh, A. Self-assembled gelators for organic electronics. *Angew. Chem., Int. Ed.* **2012**, *51*, 1766–1776.
- (10) Yang, X.; Zhang, G.; Zhang, D. Stimuli responsive gels based on low molecular weight gelators. *J. Mater. Chem.* **2012**, *22*, 38–50.
- (11) Zhang, L.; Li, S.; Squillaci, M. A.; Zhong, X.; Yao, Y.; Orgiu, E.; Samori, P. Supramolecular Self-Assembly in a Sub-micrometer Electrode Cavity: Fabrication of Heat-Reversible pi-Gel Memristor. *J. Am. Chem. Soc.* **2017**, *139*, 14406–14411.
- (12) Draper, E. R.; Adams, D. J. Photoresponsive gelators. *Chem. Commun.* **2016**, *52*, 8196–8206.
- (13) Sun, Z.; Huang, Q.; He, T.; Li, Z.; Zhang, Y.; Yi, L. Multistimuli-responsive supramolecular gels: design rationale, recent advances, and perspectives. *Chem. Phys. Chem.* **2014**, *15*, 2421–2430.
- (14) Yan, X.; Wang, F.; Zheng, B.; Huang, F. Stimuli-responsive supramolecular polymeric materials. *Chem. Soc. Rev.* **2012**, *41*, 6042–6065.
- (15) Zhang, J.; Su, C.-Y. Metal-organic gels: From discrete metallogelators to coordination polymers. *Coord. Chem. Rev.* **2013**, *257*, 1373–1408.
- (16) Fages, F. Metal coordination to assist molecular gelation. *Angew. Chem., Int. Ed.* **2006**, *45*, 1680–1682.
- (17) Tam, A. Y.-Y.; Yam, V. W.-W. Recent advances in metallogels. *Chem. Soc. Rev.* **2013**, *42*, 1540–1567.
- (18) Dastidar, P.; Ganguly, S.; Sarkar, K. Metallogels from Coordination Complexes, Organometallic, and Coordination Polymers. *Chem. – Asian J.* **2016**, *11*, 2484–2498.
- (19) Gasnier, A.; Royal, G.; Terech, P. Metallo-supramolecular gels based on a multitopic cyclam bis-terpyridine platform. *Langmuir* **2009**, *25*, 8751–8762.

- (20) Kotova, O.; Daly, R.; dos Santos, C. M. G.; Boese, M.; Kruger, P. E.; Boland, J. J.; Gunnlaugsson, T. Europium-directed self-assembly of a luminescent supramolecular gel from a tripodal terpyridine-based ligand. *Angew. Chem., Int. Ed.* **2012**, *51*, 7208–7212.
- (21) Escuder, B.; Rodríguez-Llansola, F.; Miravet, J. F. Supramolecular gels as active media for organic reactions and catalysis. *New J. Chem.* **2010**, *34*, 1044–1054.
- (22) Wang, X.; Han, Y.; Liu, Y.; Zou, G.; Gao, Z.; Wang, F. Cooperative Supramolecular Polymerization of Fluorescent Platinum Acetylides for Optical Waveguide Applications. *Angew. Chem., Int. Ed.* **2017**, *56*, 12466–12470.
- (23) Zhang, J.-J.; Lu, W.; Sun, R. W.-Y.; Che, C.-M. Organogold(III) supramolecular polymers for anticancer treatment. *Angew. Chem., Int. Ed.* **2012**, *51*, 4882–4886.
- (24) Wang, J.; Chen, Y.; Law, Y.-C.; Li, M.; Zhu, M.-X.; Lu, W.; Chui, S. S.-Y.; Zhu, N.; Che, C. M. Organo- and hydrogelators based on luminescent monocationic terpyridyl platinum(II) complexes with biphenylacetylide ligands. *Chem. – Asian J.* **2011**, *6*, 3011–3019.
- (25) Anthony Yiu-Yan Tam, K. M.-C. W.; Yam, V. W.-W. Unusual Luminescence Enhancement of Metalloids of Alkynylplatinum(II) 2,6-Bis(N-alkylbenzimidazol-2'-yl)pyridine Complexes upon a Gel-to-Sol Phase Transition at Elevated Temperatures. *J. Am. Chem. Soc.* **2009**, *131*, 6253–6260.
- (26) Tam, A. Y.-Y.; Wong, K. M.-C.; Yam, V. W.-W. Influence of counteranion on the chiral supramolecular assembly of alkyneplatinum(II) terpyridyl metalloids that are stabilized by Pt...Pt and pi-pi interactions. *Chem. – Eur. J.* **2009**, *15*, 4775–4778.
- (27) Tam, A. Y.-Y.; Wong, K. M.-C.; Zhu, N.; Wang, G.; Yam, V. W. Luminescent alkyneplatinum(II) terpyridyl metalloids stabilized by Pt...Pt, pi-pi, and hydrophobic-hydrophobic interactions. *Langmuir* **2009**, *25*, 8685–8695.
- (28) Au, V. K.-M.; Zhu, N.; Yam, V. W.-W. Luminescent metalloids of bis-cyclometalated alkynegold(III) complexes. *Inorg. Chem.* **2013**, *52*, 558–567.
- (29) Tam, A. Y.-Y.; Wong, K. M.-C.; Wang, G.; Yam, V. W.-W. Luminescent metalloids of platinum(II) terpyridyl complexes: interplay of metal...metal, pi-pi and hydrophobic-hydrophobic interactions on gel formation. *Chem. Commun.* **2007**, 2028–2030.
- (30) Camerel, F.; Ziessel, R.; Donnio, B.; Bourgoigne, C.; Guillon, D.; Schmutz, M.; Iacovita, C.; Bucher, J. P. Formation of gels and liquid crystals induced by PtPt and pi-pi* interactions in luminescent sigma-alkynyl platinum(II) terpyridine complexes. *Angew. Chem., Int. Ed.* **2007**, *46*, 2659–2662.
- (31) Wu, H.; Zheng, J.; Kjoniksen, A. L.; Wang, W.; Zhang, Y.; Ma, J. Metalloids: Availability, Applicability, and Advanceability. *Adv. Mater.* **2019**, *31*, 1806204.
- (32) Luo, L.; Benameur, A.; Brignou, P.; Choi, S. H.; Rigaut, S.; Frisbie, C. D. Length and Temperature Dependent Conduction of Ruthenium-Containing Redox-Active Molecular Wires. *J. Phys. Chem. C* **2011**, *115*, 19955–19961.
- (33) Meng, F.; Hervault, Y. M.; Shao, Q.; Hu, B.; Norel, L.; Rigaut, S.; Chen, X. Orthogonally modulated molecular transport junctions for resettable electronic logic gates. *Nat. Commun.* **2014**, *5*, 3023.
- (34) Schwarz, F.; Kastlunger, G.; Lissel, F.; Egler-Lucas, C.; Semenov, S. N.; Venkatesan, K.; Berke, H.; Stadler, R.; Lortscher, E. Field-induced conductance switching by charge-state alternation in organometallic single-molecule junctions. *Nat. Nanotechnol.* **2016**, *11*, 170–176.
- (35) Tanaka, Y.; Kato, Y.; Sugimoto, K.; Kawano, R.; Tada, T.; Fujii, S.; Kiguchi, M.; Akita, M. Single-molecule junctions of multinuclear organometallic wires: long-range carrier transport brought about by metal–metal interaction. *Chem. Sci.* **2021**, *12*, 4338–4344.
- (36) Milan, D. C.; Vezzoli, A.; Planje, I. J.; Low, P. J. Metal bis(acetylide) complex molecular wires: concepts and design strategies. *Dalton Trans.* **2018**, *47*, 14125–14138.
- (37) Naher, M.; Bock, S.; Langtry, Z. M.; O'Malley, K. M.; Sobolev, A. N.; Skelton, B. W.; Korb, M.; Low, P. J. Synthesis, Structure and Physical Properties of “Wire-like” Metal Complexes. *Organometallics* **2020**, *39*, 4667–4687.
- (38) Zhang, L.-Y.; Duan, P.; Wang, J.-Y.; Zhang, Q.-C.; Chen, Z.-N. Ruthenium(II) as Conductive Promoter To Alleviate Conductance Attenuation in Oligoynyl Chains. *J. Phys. Chem. C* **2019**, *123*, 5282–5288.
- (39) Wuttke, E.; Pevny, F.; Hervault, Y. M.; Norel, L.; Drescher, M.; Winter, R. F.; Rigaut, S. Fully delocalized (ethynyl)(vinyl)phenylene bridged triruthenium complexes in up to five different oxidation states. *Inorg. Chem.* **2012**, *51*, 1902–1915.
- (40) Ou, Y. P.; Zhang, J.; Zhang, M. X.; Zhang, F.; Kuang, D.; Hartl, F.; Liu, S. H. Bonding and Electronic Properties of Linear Diethynyl Oligoethenoacene-Bridged Diruthenium Complexes and Their Oxidized Forms. *Inorg. Chem.* **2017**, *56*, 11074–11086.
- (41) Ying, J. W.; Liu, I. P.-C.; Xi, B.; Song, Y.; Campana, C.; Zuo, J. L.; Ren, T. Linear trimer of diruthenium linked by butadiyn-diyl units: a unique electronic wire. *Angew. Chem., Int. Ed.* **2010**, *49*, 954–957.
- (42) Mulas, A.; Hervault, Y. M.; He, X.; Di Piazza, E.; Norel, L.; Rigaut, S.; Lagrost, C. Fast Electron Transfer Exchange at Self-Assembled Monolayers of Organometallic Ruthenium(II) σ -Arylacetylide Complexes. *Langmuir* **2015**, *31*, 7138–7147.
- (43) Colombo, A.; Dragonetti, C.; Roberto, D.; Ugo, R.; Falciola, L.; Luzzati, S.; Kotowski, D. A Novel Diruthenium Acetylide Donor Complex as an Unusual Active Material for Bulk Heterojunction Solar Cells. *Organometallics* **2011**, *30*, 1279–1282.
- (44) Roberts, R. L.; Schwich, T.; Corkery, T. C.; Cifuentes, M. P.; Green, K. A.; Farmer, J. D.; Low, P. J.; Marder, T. B.; Samoc, M.; Humphrey, M. G. Organometallic Complexes for Nonlinear Optics. 45. Dispersion of the Third-Order Nonlinear Optical Properties of Triphenylamine-Cored Alkynylruthenium Dendrimers. *Adv. Mater.* **2009**, *21*, 2318–2322.
- (45) Simpson, P. V.; Watson, L. A.; Barlow, A.; Wang, G.; Cifuentes, M. P.; Humphrey, M. G. Record Multiphoton Absorption Cross-Sections by Dendrimer Organometalation. *Angew. Chem., Int. Ed.* **2016**, *55*, 2387–2391.
- (46) Samoc, M.; Morrall, J. P.; Dalton, G. T.; Cifuentes, M. P.; Humphrey, M. G. Two-photon and three-photon absorption in an organometallic dendrimer. *Angew. Chem., Int. Ed.* **2007**, *46*, 731–733.
- (47) Zhang, X.; Shi, L.; Fox, M. A.; Barlow, A.; Morshedi, M.; Cifuentes, M. P.; Humphrey, M. G.; Mongin, O.; Paul, F.; Paul-Roth, C. O. Nonlinear optical properties of meso-Tetra(fluorenyl)porphyrins peripherally functionalized with one to four ruthenium alkyne substituents. *Dyes Pigm.* **2021**, *188*, 109155.
- (48) Triadon, A.; Grelaud, G.; Richy, N.; Mongin, O.; Moxey, G. J.; Dixon, I. M.; Yang, X.; Wang, G.; Barlow, A.; Rault-Berthelot, J.; Cifuentes, M. P.; Humphrey, M. G.; Paul, F. Linear and Third-Order Nonlinear Optical Properties of Fe(η^5 -C5Me5)(κ^2 -dppe)- and trans-Ru(κ^2 -dppe)2-Alkynyl Complexes Containing 2-Fluorenyl End Groups. *Organometallics* **2018**, *37*, 2245–2262.
- (49) Norel, L.; Di Piazza, E.; Feng, M.; Vacher, A.; He, X.; Roisnel, T.; Maury, O.; Rigaut, S. Lanthanide Sensitization with Ruthenium Carbon-Rich Complexes and Redox Commutation of Near-IR Luminescence. *Organometallics* **2014**, *33*, 4824–4835.
- (50) Al Sabea, H.; Norel, L.; Galangau, O.; Hijazi, H.; Metivier, R.; Roisnel, T.; Maury, O.; Bucher, C.; Riobe, F.; Rigaut, S. Dual Light and Redox Control of NIR Luminescence with Complementary Photochromic and Organometallic Antennae. *J. Am. Chem. Soc.* **2019**, *141*, 20026–20030.
- (51) Norel, L.; Bernot, K.; Feng, M.; Roisnel, T.; Caneschi, A.; Sessoli, R.; Rigaut, S. A carbon-rich ruthenium decorated dysprosium single molecule magnet. *Chem. Commun.* **2012**, *48*, 3948–3950.
- (52) Vives, G.; Tour, J. M. Synthesis of a nanocar with organometallic wheels. *Tetrahedron Lett.* **2009**, *50*, 1427–1430.
- (53) Kadjane, P.; Starck, M.; Camerel, F.; Hill, D.; Hildebrandt, N.; Ziessel, R.; Charbonniere, L. J. Divergent approach to a large variety of versatile luminescent lanthanide complexes. *Inorg. Chem.* **2009**, *48*, 4601–4603.
- (54) Camerel, F.; Donnio, B.; Bourgoigne, C.; Schmutz, M.; Guillon, D.; Davidson, P.; Ziessel, R. Tuning the thermotropic and lyotropic properties of liquid-crystalline terpyridine ligands. *Chem. – Eur. J.* **2006**, *12*, 4261–4274.

(55) Céline Olivier, B. K.; Touchard, D.; Rigaut, S. Redox-Active Molecular Wires Incorporating Ruthenium(II) σ -Arylacetylide Complexes for Molecular Electronics. *Organometallics* **2008**, *27*, 509–518.

(56) Camerel, F.; Ulrich, G.; Ziessel, R. New Platforms Integrating Ethynyl-Grafted Modules for Organogels and Mesomorphic Superstructures. *Org. Lett.* **2004**, *6*, 4171–4174.

(57) Zhang, J.; Xu, X.-D.; Chen, L.-J.; Luo, Q.; Wu, N.-W.; Wang, D.-X.; Zhao, X.-L.; Yang, H.-B. Platinum Acetylide Complexes Containing Iptycene as Cores: A New Family of Unexpected Efficient Organometallic Gelators. *Organometallics* **2011**, *30*, 4032–4038.

(58) Falivene, L.; Cao, Z.; Petta, A.; Serra, L.; Poater, A.; Oliva, R.; Scarano, V.; Cavallo, L. Towards the online computer-aided design of catalytic pockets. *Nat. Chem.* **2019**, *11*, 872–879.

(59) Mabesoone, M. F. J.; Palmans, A. R. A.; Meijer, E. W. Solute-Solvent Interactions in Modern Physical Organic Chemistry: Supramolecular Polymers as a Muse. *J. Am. Chem. Soc.* **2020**, *142*, 19781–19798.